Commonalities and evolutionary divergences of mandible shape ontogenies in rodents.

Morgane Dubied, Sophie Montuire, Nicolas Navarro

Commonalities and evolutionary divergences of mandible shape ontogenies in rodents

Running title: **Evolution of postnatal ontogenies in rodents**

Morgane Dubied[1], Sophie Montuire[1,2], Nicolas Navarro[1,2]
[1]Biogeosciences, UMR 6282 CNRS, EPHE, Université Bourgogne Franche-Comté, 6 bd Gabriel, 21000 Dijon
[2]EPHE, PSL University, 75014 Paris

Email
morgane.dubied@u-bourgogne.fr
sophie.montuire@ephe.psl.eu
nicolas.navarro@ephe.psl.eu

ORCID number
Morgane Dubied: 0000-0002-9304-2714
Sophie Montuire: 0000-0002-5341-5344
Nicolas Navarro: 0000-0001-5694-4201

Acknowledgements
We are grateful to all the curators who allowed us to study their collections: Violaine Nicolas (National Natural History Museum Paris), Loïc Costeur (Natural History Museum Basel), Olivier Pauwels (Royal Belgian Institute of Natural Sciences), Laurent Vallotton and Manuel Ruedi (Natural History Museum of Geneva). Mathilde Tissier (Hubert Curien Pluridisciplinary Institute) is also thanked for providing access to *Cricetus cricetus* specimens. We thank Lauriane Poloni (Biogéosciences) for help with CT scanning, and Remi Laffont (Biogéosciences) for help in data curation. We are grateful to Philip Cox, Vincent Debat, Lionel Hautier and Miriam Leah Zelditch for helpful comments on early versions of the manuscript. We are also grateful to Carmela Chateau-Smith for English editing. The Gismo platform and morphOptics are acknowledged for providing access to 3D scanning. This research project was supported by the AP EPHE-2019.

Author contributions
All authors contributed to the study design. MD collected species in museum and conducted the phenotyping. MD and NN analyzed the data. All authors contributed with edits and comments to analyses and wrote the manuscript.

Conflict of interest

Authors declare no conflicts of interest.

Ethical approval

All procedures on laboratory animals were approved by the local ethical committee of the University of Burgundy in Dijon (Project APAFIS#18405-2019011014262528).

Abstract

In mammals, significant changes take place during postnatal growth, linked to changes in diet (from sucking to gnawing). During this period, mandible development is highly interconnected with muscle growth and the epigenetic interactions between muscle and bone control the spatialization of bone formation and remodeling in response to biomechanical strain. This mechanism contributes to postnatal developmental plasticity, and may have influenced the course of evolutionary divergences between species and clades. We sought to model postnatal changes at a macroevolutionary scale by analyzing ontogenetic trajectories of mandible shape across 16 species belonging mainly to two suborders of Rodents, Myomorpha and Hystricomorpha, which differ in muscle attachments, tooth growth, and life-history traits. Myomorpha species present a much stronger magnitude of changes over a shorter growth period. Among Hystricomorpha, part of the observed adult shape is set up prenatally, and most postnatal trajectories are genus-specific, which agrees with non-linear developmental trajectories over longer gestational periods. Beside divergence at large scale, we find some collinearities between evolutionary and developmental trajectories. A common developmental trend was also observed, leading to enlargement of the masseter fossa during postnatal growth. The tooth growth, especially hypselodonty, seems to be a major driver of divergences of postnatal trajectories. These muscle- and tooth-related effects on postnatal trajectories suggest opportunities for developmental plasticity in the evolution of the mandible shape, opportunities that may have differed across Rodent clades.

Keywords: Rodents, geometric morphometrics, macroevolution, mandible shape, postnatal growth

Introduction

Understanding developmental mechanisms in evolution is crucial to apprehend the diversification of organismal forms (Darwin 1859, Alberch 1980, Smith et al. 1985). It is well recognized nowadays that these mechanisms lead to discontinuities and directionalities in the space of shapes (Alberch 1980, Gerber 2014, Salazar-Ciudad 2021). Indeed, they induce biases in the phenotypic outcomes of random mutations (Alberch 1982, Hallgrimsson et al. 2006, Uller et al. 2020) and therefore in the evolutionary trajectories (Uller et al. 2018, Kavanagh et al. 2013). The existence of such developmental bias results in some parallelism between developmental and evolutionary trajectories (Alberch et al. 1979, Gould 1977, Webster and Zeldicth 2005). Despite the abundant theoretical literature about the role of development in evolution (Arthur 2001, Uller 2020), there are practical problems to gather ontogenetic data at a large scale. Empirical works are still needed to assess whether directions in the morphospace supported by developmental variation are also the most evolvable. Developmental processes influence thus the phenotypic production and the availability of variation to selection, questioning the importance of evolution of the ontogenetic trajectories themselves in shaping the diversity of organismal shapes.

The evolution of ontogenetic trajectories involves a complex interplay of the rate and timing of development of the various parts constituting an organism as well as with the internal and/or external environment. During pre- and postnatal development, organismal growth responds to many genetic, biomechanical, and environmental factors. As organs grow, they compete for space and resources, while maintaining a functional phenotype under a variety of selection regimes (Dibner and Kitchell 2007, Nijhout and Emlen 1998, Olsen and Reginato 2000). In vertebrates, for example, epigenetic interactions will compensate for, and coordinate, the growth of the organs that form the head, to acquire and/or maintain functions such as occlusion between the lower and upper jaws (Hallgrimsson and Hall 2011, Lieberman 2011). Similarly, changes in muscle forces during development regulate the spatialization and intensity of bone remodeling (Herring 2011, Zelditch and Swiderski 2011, Zelditch et al. 2008), which may change not only the structure but also the shape of the bone (Martine-Maza et al. 2016). Organ interactions may drive the occurrence and intensity of developmental plasticity and the indirect response to selection (Fusco 2008). By responding to developmental changes in forces and movements, epigenetic interactions between bones and other tissues could drive morphological variation (Hallgrimsson and Hall 2011). Epigenetics could therefore structure evolutionary trajectories, potentially biasing diversification among taxa (Young and Badyaev 2007, Renvoisé et al. 2017) and thus becoming a major determinant of plasticity-led evolution (West-Eberhard 2003, Uller 2020).

Postnatal growth is a key period in mammals, during which skull variation is strongly modified (Mitteroecker and Bookstein 2009) and then stabilized (Zelditch et al. 2003). During this transition from the juvenile to the adult head, major biomechanical changes occur in response to changes in the use of the masticatory apparatus related to weaning, from sucking to gnawing and chewing movements (Curley et al. 2009). An important component of adult anatomy is the eruption and growth of teeth, in relation to the acquisition of mastication. Tooth development partly determines the complexity of the ontogenetic trajectory of the mouse mandible (Swiderski and Zelditch 2013). The ever-growing incisor leads to bone remodeling during mandible growth (Renvoisé and Montuire 2015). This simple, highly integrated, skeleton element strongly responds to changes in mechanical constraints related to food hardness (Anderson et al. 2014; Menegaz and Ravosa 2017), or to muscle dystrophy (Renaud et al. 2010). The mandible is an ideal model system to observe organ interactions, and thus to test their evolutionary consequences, as its development is tightly integrated with that of teeth and muscles (Atchley 1993, Klingenberg and Navarro 2012).

Rodentia is a very diverse and disparate mammal order, in which postnatal changes can be observed on a large scale. The muscle attachment to the cranium is used to classify rodents into three main suborders: Myomorpha, Sciuromorpha, and Hystricomorpha (Hautier 2010, Hautier et al. 2008, Simpson 1945, Wood 1965). The mandible presents a wide variety of forms across these suborders (Hautier et al. 2011), which group into two mandibular structures (Tullberg, 1899): hystricognaths (with a strong inwardly projecting angular process and an outwardly projecting condyloid process) or sciurognaths (with an outwardly projecting angular process and an inwardly projecting condyloid process). The insertions of the masseter muscles to the mandible and the cranium were used by early authors (Brandt 1855, Wood 1965) to describe four different morphologies across rodents: protrogomorphy (small to medium infraorbital foramen, a reduced masseter and a predominant temporalis), sciuromorphy (very small infraorbital foramen and a lateral masseter inserted in the anterior part of the orbital arch), hystricomorphy (infraorbital foramen is very developed and almost circular) and myomorphy (infraorbital foramen is narrow at the base and widened in its upper part). Rodents present also three main types of molar growth (Renvoisé and Montuire 2015): root apex closed after tooth maturation (brachyodonty), ever-growing with open root (hypsodonty), or with no root (hypselodonty); and molars take up a great deal of space in the mandible as they develop, particularly in hypselodont species.

Beyond intricate interconnections with postnatal developing structures (muscles and tooth), shape disparity of the mandible seems to be generated prenatally, at least in Sciuridae, with compensated postnatal ontogenetic variations (Zelditch et al. 2016), suggesting a relatively reduced role for biomechanical plasticity in the establishment of species differences. Data supporting this result include most species belonging to the Sciuridae, which is relatively conservative in terms of skull shape (Cardini and Thoringhton 2006). Myomorpha and Hystricomorpha are diversified in shape, probably because of their high diversification rate and high diversity (Alhajeri and Steppan 2018; Wilson 2013). Therefore, studying the evolution of their ontogenies will likely provide additional contrasts to better understand the importance of postnatal growth in the set-up of species divergences.

These two suborders and the evolution of their ontogenies will be the focus of this study, mainly because they exhibit diverse life-history traits among species (Wilson et al. 2016; Wolff and Sherman 2008). Gestation and weaning are shorter in Myomorpha, which generally give birth to large litters many times a year. This behavior involves a short *in-utero* development and a rapid and therefore mechanically brutal weaning (Curley et al. 2009). Hystricomorpha give birth to small litters a few times a year. Parental care is therefore different, with longer behavioral weaning and less brutal dietary weaning, over a much longer period (Wolff and Sherman 2008). The potential for postnatal plasticity could likely be different between the two suborders. A wide variety of diets is also found within these two groups (Nowak 1999). Changes in diet might correlate with evolutionary changes in muscle attachment, direction of mastication, and mandible shape (Alvarez and Pérez 2019).

Geometric morphometrics is used to describe postnatal trajectories of the mandible shape on specifically collected species with identified juveniles (before weaning), instead of using static allometry from a series of specimens varying in size. Comparing these postnatal growths within and between Myomorpha and Hystricomorpha suborders—together with two Sciuromorpha species for comparison— will provide valuable data about the influences of development in evolution, for instance if evolutionary and developmental directions in the morphospace coincide (Erwin 2007, Gerber 2014, Wilson 2013, Zelditch et al. 2016). It will also provide data about the evolution of ontogenesis in rodents, if these evolutionary changes sustain species divergences, and if postnatal growth is a key period for the establishment of adult disparity. Contrasting the variation in these mandible shape trajectories to life-history traits and to the development of muscles and teeth will

underline the importance of the development of these traits in the evolution of the mandible ontogenesis.

Materials and methods

SPECIMENS

Specimens were selected from five different collections: the Royal Belgian Institute of Natural Sciences (IRSNB), the Natural History Museum Geneva (MHNG), the National Museum of Natural History Paris (MNHN), the Natural History Museum Basel (NMB) and the Biogéosciences Laboratory, Dijon (Table S1). *Mesocricetus auratus* (RjHan:AURA), *Meriones unguiculatus* (Crl:MON) and *Mus musculus* (BALB/c) are laboratory individuals raised at the University of Burgundy (Project APAFIS#18405-2019011014262528) for which the age of each individual is known (7 days for juveniles). Juvenile specimens from Museum collections were carefully checked for their putative age with these following criteria about tooth eruption and ossification, which correspond to the observed characteristics made on laboratory 7 day-old juveniles. Molars' occlusal surface is just emerged from the bone and incisors are barely emerged as well. The ossification of mandibular processes is poor (presence of cartilage at the top of the postcondylar process) and the one of the cranium is incomplete (cartilage between the bones constituting the cranium). It results that a large number of registered juveniles were disregarded to keep only undoubtful early juveniles. The final data set for this study includes 105 hemimandibles attributed to 16 species: five for Myomorpha, eight for Hystricomorpha, two for Sciuromorpha, and *Oryctolagus cuniculus* (Lagomorpha) as the outgroup species (Fig. 1). Only one hemimandible per specimen was used, chosen by state of preservation. For the purpose of checking the effect of the age of juveniles, 27 additional specimens were also sampled and added as supplementary data. They represented 15 days old juveniles of Myomorpha species raised in the lab and a few juveniles of *Microtus arvalis* older than one week.

Mandibles shorter than 5 cm in length were scanned by µCT-scan (Bruker Skyscan 1174) and reconstructed using Avizo®9.2 (FEI systems). Those longer than 5 cm were scanned with a Shining 3D® Einscan Pro surface scanner. One specimen was processed on the two acquisition pipelines and digitized several times. Preliminary analysis identified no spurious variation in these replicates. Before landmark digitization, 3D models were decimated to 200 000 faces, using the *Rvcg* R package 0.18 (Schlager 2017).

LIFE HISTORY

Data about dental development (Ungar 2010), and ecology such as reproductive traits (Wilson et al. 2016; De Magalhaes and Costa 2009), were gathered from the literature.

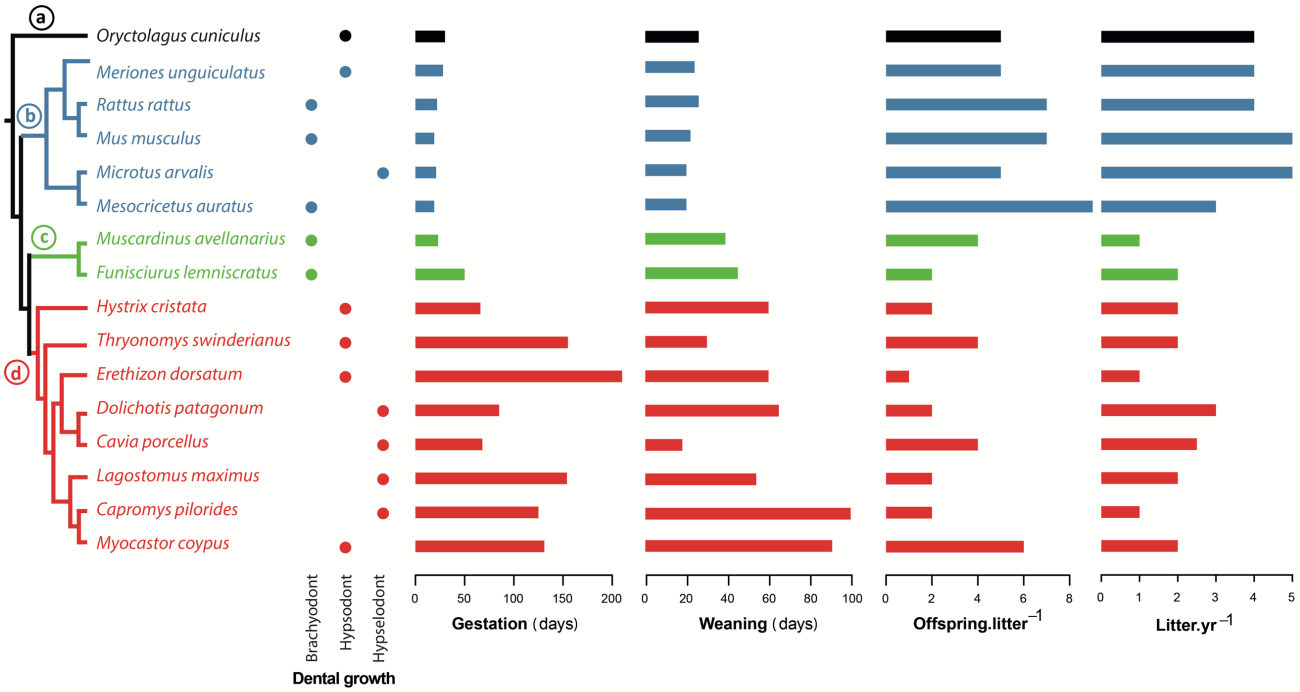

Figure **1.** Summary of data on phylogeny, tooth growth (Ungar 2010) and reproductive traits (gestational duration, weaning time and offspring by litter) for the species sampled for the study (Wilson et al. 2016, De Magalhaes and Costa 2009). Color code for outgroup and suborders: a) Lagomorpha in black; b) Myomorpha in blue; c) Sciuromorpha in green; d) Hystricomorpha in red.

In summary (Fig. 1), gestational duration varies considerably, three to nine times shorter for Myomorpha (19 to 22 days, median = 20), than for Hystricomorpha (66 to 210 days, median = 125). A similar difference is also observed for weaning time, which occurs in Myomorpha between 20 and 26 days after birth (median = 22), while it occurs from 18 to 100 days after birth (median = 60) in Hystricomorpha. The two suborders have a similar number of litters per year (a maximum of five), but on average Myomorpha have four litters per year, while Hystricomorpha have only two. About the skull structure, all species belonging to Myomorpha and Hystricomorpha are either myomorphous or hystricomorphous respectively. Sciuromorpha species are either sciuromorphous (*Funisciurus lemniscratus*) or myomorphous (*Muscardinus avellanarius*). All species are sciurognaths except the Hystricomorpha species, which are hystricognaths.

LANDMARKS AND SEMILANDMARKS

Ten landmarks were digitized, together with 33 semilandmarks divided into three curves (with 4 on the coronoid process, 9 along the lunar notch, and 10 between postcondylar and angular processes; Fig. 2) using the *Digit3DLand* R package 0.1.3 (Laffont and Navarro 2019). Semilandmarks were slid along their tangent by minimizing the bending energy, and back-projected on the 3D curves (Gunz et al. 2005).

DATA ANALYSIS

Procrustes alignment, checked for approximation and imbalance effects

Landmarks and sliding semilandmarks were superimposed using a full generalized Procrustes analysis (GPA) with the *Morpho* R package 2.8 (Schlager 2017). Tangent space approximation of distances between specimens was checked against Riemannian distance, which has been shown to

be generally accurate across studies encompassing a variety of taxa and taxonomic ranges (Klingenberg 2020), including mammalian orders (Marcus et al. 2000). The reference shape on which landmark conformations are aligned is known to structure variation in the tangent space, thus determining any distortion of distances between individuals (Bookstein 2016). As developmental stages and species were not equally sampled or equally represented between clades, we also checked whether aligning landmark conformations on a weighted average rather than on the grand mean (the usual method) still provides consistent results. The average from each developmental stage of each clade (weighting species in the clade equally) was therefore used as reference shape in a new Procrustes superimposition. The angle between this weighted mean shape and the original mean shape was computed and compared to the angles observed between any two specimens. The Lagomorphs were aligned only as supplementary data.

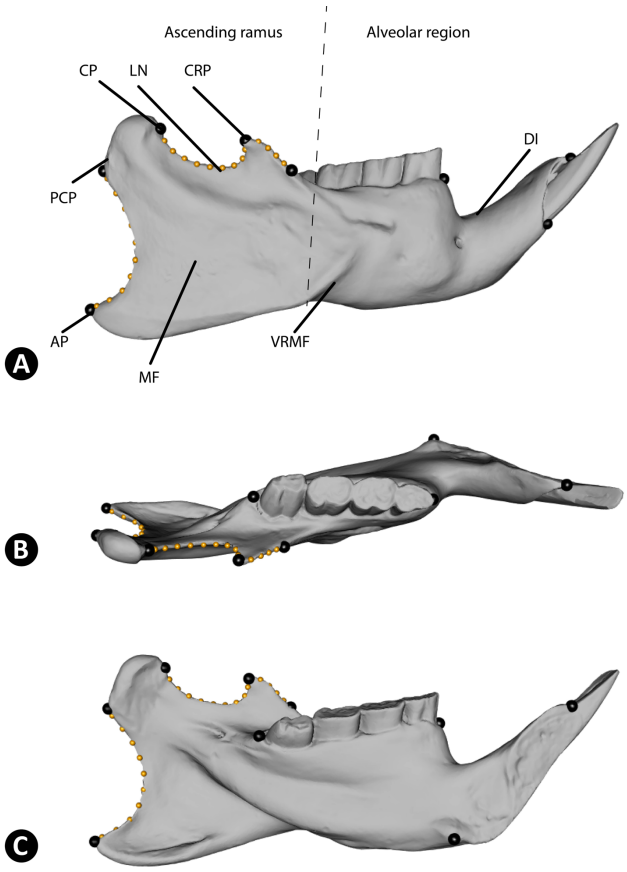

Figure **2.** Landmarks and semilandmarks on 3D mandibular surface. Black dots are manual 3D landmarks, and small yellow dots represent the semilandmark template. (AP: angular process, CP: condylar process, DI: diastema, CRP: coronoid process, LN: lunar notch, MF: masseter fossa, PCP: postcondylar process, VRMF: ventral ridge of masseter fossa). A: labial view; B: occlusal view; C: lingual view.

Developmental, phylogenetic-aligned and postnatal morphospaces

A developmental morphospace, the embedding of both juveniles and adults in the same morphospace (Eble et al. 2003), was obtained by applying principal component analysis (PCA) to the covariance matrix of the tangent coordinates. This morphospace maximizes shape variation in directions that describe either developmental changes, evolutionary changes or both simultaneously. To compare the developmental structuration of the morphospace and evolutionary divergences, a

phylogenetically aligned morphospace was also computed based on the principal component ordination of the phylogenetic covariance matrix $\boldsymbol{C}$ (Collyer and Adams 2021). The phylogenetic covariance matrix $\boldsymbol{C}$ was computed according to a Brownian-motion model of evolutionary divergence. This space (PaPCs) maximizes variation in directions that describe evolutionary divergences. This analysis was done with the *geomorph* R package 3.2.1 (Adams et al. 2016). To observe the structuration of the variation of the postnatal trajectories alone, a PCA was performed on the covariance matrix of the vectors $\boldsymbol{z}$ of differences between juvenile and adult shape averages $\boldsymbol{y}$ of each species. These vectors are the average shape changes occurring during postnatal growth. Scaling these vectors by the difference between juvenile and adult average sizes would have led to a rough estimate of allometric vectors. As Hystricomorpha species are much larger than other species, rescaling would have resulted in trivial size differences.

A tree pruned for the species present in the sample (Wilson et al. 2016) was built with the *ape* R package 5.3 (Paradis and Schliep, 2019), and was projected onto the different morphospaces, using the *phytools* R package 0.7-20 (Revell 2012), to observe their phylogenetic structuration.

Ancestral postnatal trajectories, common pattern of growth and evolutionary changes

The phylogenetic mean of postnatal trajectories was computed according to the generalized least-squares estimator $\bar{\boldsymbol{z}}_{pgls} = (\mathbf{1}'\boldsymbol{C}^{-1}\mathbf{1})^{-1}\mathbf{1}'\boldsymbol{C}^{-1}\boldsymbol{z}$ (Rohlf 2001, Revell 2009), with $\boldsymbol{z}$ the vectors of shape changes between juveniles and adults and $\boldsymbol{C}$ the phylogenetic covariance matrix. This estimate corresponds to the value at the root of the tree (Rohlf 2001). The $\boldsymbol{z}$ vectors correspond to postnatal shape changes, $\bar{\boldsymbol{z}}_{pgls}$ estimates the ancestral pattern of shape changes during postnatal growth according to Brownian motion. Estimate of the postnatal trajectory for each suborder was computed as the least-squares (LS) means $\hat{\boldsymbol{z}} = \boldsymbol{L}\boldsymbol{\beta}$, with $\boldsymbol{L}$ the matrix corresponding to the linear contrast for the suborder, and $\boldsymbol{\beta} = (\boldsymbol{X}'\boldsymbol{C}^{-1}\boldsymbol{X})^{-1}\boldsymbol{X}'\boldsymbol{C}^{-1}\boldsymbol{z}$, the phylogenetic generalized least-squares estimates of suborder differences.

To check the alignment of the principal directions of the morphospace (developmental or phylogenetically-aligned) with the phylogenetic mean postnatal trajectory $\bar{\boldsymbol{z}}_{pgls}$, or with the suborder estimates of postnatal trajectories $\hat{\boldsymbol{z}}$, angles between these estimates and the shape features described by PCs were estimated as $\theta = cos^{-1}(\boldsymbol{v}_i \cdot \boldsymbol{v}_j)$ (Klingenberg 1998, Zelditch et al. 2004), with the normalized vectors $\boldsymbol{v}$ being either eigenvectors or normalized trajectories to unit length. The probability that the angle between two random vectors is lower than the observed angle was estimated as the area of the cap of a hypersphere defined by this angle (Li 2011), and computed with the *Morpho* R package 2.8 (Schlager 2017). Approximation of standard errors on angles based on $\hat{\boldsymbol{z}}$ were computed based on the sampling distribution of $\boldsymbol{\beta}$ (Meyer and Houle 2013, Houle and Meyer 2015), and according to $\boldsymbol{z}^* \sim N(\hat{\boldsymbol{z}}, \mathbf{S}_e \otimes \boldsymbol{L}(\boldsymbol{X}'\boldsymbol{C}^{-1}\boldsymbol{X})^{-1}\boldsymbol{L}')$, where $\mathbf{S}_e$ is the residual covariance matrix, and $\otimes$ stands for the Kronecker product. Descriptive statistics on sampled angles were computed with the *circular* R package 0.4-93 (Agostinelli and Lund 2017).

The angle between phylogenetically aligned variation (PaPCA) and the average directions of postnatal changes ($\bar{\boldsymbol{z}}_{pgls}$ and $\hat{\boldsymbol{z}}$) was measured as $\delta_i = cos^{-1}\{(\boldsymbol{v}_i^t\boldsymbol{L}\boldsymbol{L}^t\boldsymbol{v}_i)^{0.5}\}$ with $\boldsymbol{L}_{3k \times q}$ the matrix of q eigenvectors from the PaPCA, where q was set equal to half the divergence dimensionality ($q = 7$) and $\boldsymbol{v}$ the normalized postnatal vectors (Krzanowski 1979). To assess more formally the degree of independence between developmental trajectories and evolutionary divergences, a common spectral decomposition of the two matrices was performed (Krzanowski 1979). This approach captures the overall similarity from the eigen decomposition of $\boldsymbol{H} = \sum_{i=1}^{p} \boldsymbol{L}_i\boldsymbol{L}_i^t$ where $\boldsymbol{L}$ is the matrix of the *q* first eigenvectors of either the divergences or the postnatal changes. The eigenvalues close to the maximum of *p* (here *p* = 2) means that the evolutionary or postnatal changes could be inferred from a linear combination of the eigenvectors of the other. Similarly to above, an angle δ_i could be

defined to estimate how similar an eigenvector of $\boldsymbol{H}$ is to the evolutionary or postnatal changes (Krzanowski 1979).

Comparison of juvenile and adult disparities

Even if some evolutionary divergences arise in the directions of postnatal growth, adult disparity may or not increase compared to juvenile disparity as changes in the amount or direction could be compensated and finally most of the disparity could be established prenatally as suggested for Sciuridae (Zelditch et al. 2016). Disparity levels between developmental stages of Myomorpha and Hystricomorpha were calculated as the Procrustes variance, i.e., the sum of squared Euclidean distances in the tangent space between species means $\boldsymbol{y}$ and their average divided by the number of species in the group (Zelditch et al. 2004, Drake and Klingenberg 2010). Bootstrapping of species means was used to estimate standard errors on disparity (Efron 1979, Foote 1994, Navarro 2003). Disparities were also computed on a sequence including successive principal components (PCs) defining the developmental morphospace. This sequence was used to show how taxa spread over the morphospace as defined by the main patterns of shape differentiation among species and developmental stages. Comparison of disparity between the two suborders also assessed whether evolvability varies across anatomies and modes of development.

Evolution of postnatal trajectories

The degree of phylogenetic signal in the postnatal vectors $\boldsymbol{z}$ was assessed relative to their expectation given a Brownian evolution, using the multivariate version of the *K* statistics (Adams 2014), with 10 000 simulations. The K_{mult} was computed with the *geomorph* R package 3.2.1 (Adams et al. 2016). This package also returns effect size as the z-score standardization of the K_{mult} statistics, given its distribution under the null obtained from simulation. For comparison, the phylogenetic signal was also computed separately for juvenile and for adult shapes.

To assess whether *postnatal trajectories* have evolved between suborders, the differences between suborder estimates $\hat{\boldsymbol{z}}$ with regard to their magnitude or direction of postnatal shape changes were computed. Standard errors on angles were approximated using $\boldsymbol{z}^*$sampling as explained above. Evolutionary divergence in the magnitude of shape changes occurring after birth between the Myomorpha and Hystricomorpha was evaluated from the LS-means contrast of the Euclidean length of the suborder trajectories $\left\|\hat{\boldsymbol{z}}_{myo}\right\| - \left\|\hat{\boldsymbol{z}}_{hys}\right\|$, with a *t* test using approximate standard error based on $\boldsymbol{z}^*$ sampling and the residual degree of freedom of the linear model.

Approximately phylogeny-corrected postnatal changes were computed as $\boldsymbol{z}_c = \boldsymbol{D}^{-1}\boldsymbol{z}$ (Arnold 1981, Schabenberger and Gotway 2017), where $\boldsymbol{z}$ is the vector of shape changes between juveniles and adults of each species and $\boldsymbol{D}^{-1}$ is the inverse square root of the phylogenetic covariance matrix $\boldsymbol{C}$. To obtain $\boldsymbol{D}^{-1}$, the eigen decomposition of $\boldsymbol{C}$ was used as $\boldsymbol{D}^{-1} = \boldsymbol{U}\boldsymbol{\Lambda}^{-0.5}\boldsymbol{U}'$, with $\boldsymbol{U}$ the matrix of eigenvectors, and $\boldsymbol{\Lambda}$ the diagonal matrix of eigenvalues of $\boldsymbol{C}$. Their angles with the ancestral growth $\bar{\boldsymbol{z}}_{pgls}$ was measured to assess the degree of divergences from the root of the tree. The pairwise angles between these trajectories within suborders were computed to assess the remaining variation between species once Brownian divergence is factored in, variation that could have resulted from evolutionary divergence from other traits such as life history traits. This question was evaluated more formally using a phylogenetic generalized least-squares analysis (pGLS) with the effects of tooth growth and reproductive traits on postnatal shape changes $\boldsymbol{z}$. Considering the number of species sampled and differentiation between and within Myomorpha and Hystricomorpha, traits could be strongly aggregated (Adams and Collyer 2018). Correlations between phylogeny and life history traits were first checked using two-block partial least-squares (Rohlf and Corti 2000), following the approach of Adams and Collyer (2018). Because of the strong clustering of gestational and weaning

duration and their resulting high correlation with phylogeny, they were pooled within suborders before being analyzed. Significance of the Procrustes sum of squares was evaluated using 10 000 residual permutations with the *RRPP* R package 0.5.2 (Collyer and Adams 2018). Residual permutations appear to control the family-wise error rate, even for small trees and for large isotropic dimensionalities, and to reach high power (Collyer and Adams 2018, Adams and Collyer 2018). Two points should however be noted: the sample size used here is smaller than the minimum size in these studies; the simulation scheme used by these authors did not acknowledge the peculiarities of isotropy in the tangent space where correlations between coordinates exist due to the Procrustes superimposition (Bookstein 2016; Klingenberg 2020). The family-wise error rate and power given the characteristics of the data (i.e., tree and mean shape) were computed for a continuous covariate, a three-state covariate, and a binary classification. Covariates and shapes evolve according to a Brownian model and to Procrustes constraints on the tangent space. Simulation results are provided as supplementary materials.

Visualization of shape changes

Shape effects were visualized on two meshes, corresponding to the mean shape for Myomorpha, and then for Hystricomorpha, because of the considerable anatomical differences between the two suborders. Meshes were deformed in relation to shape effect, using thin plate spline with the *Morpho* R package 2.8 (Schlager 2017). Deformations were either colorized in relation to the signed distance between the predicted and reference meshes or visualized as animated deformations, which are provided as supplementary movies.

Results

Checking tangent space approximation and imbalance effects

Correlation between Euclidean distances in the tangent space and Riemannian distances was very high (r = 0.999), confirming the accuracy of the approximation. The mean shape of Myomorpha and Hystricomorpha was very similar to the mean shape based on weighted averages ($\alpha = 2.55°$), and angles between specimens were always larger than this angle, suggesting that the shape space was ideally projected for the sample studied, and was not affected by the imbalance between the suborders. It should be recalled here that the lagomorph was aligned as supplementary data only.

Developmental and evolutionary patterns of shape changes

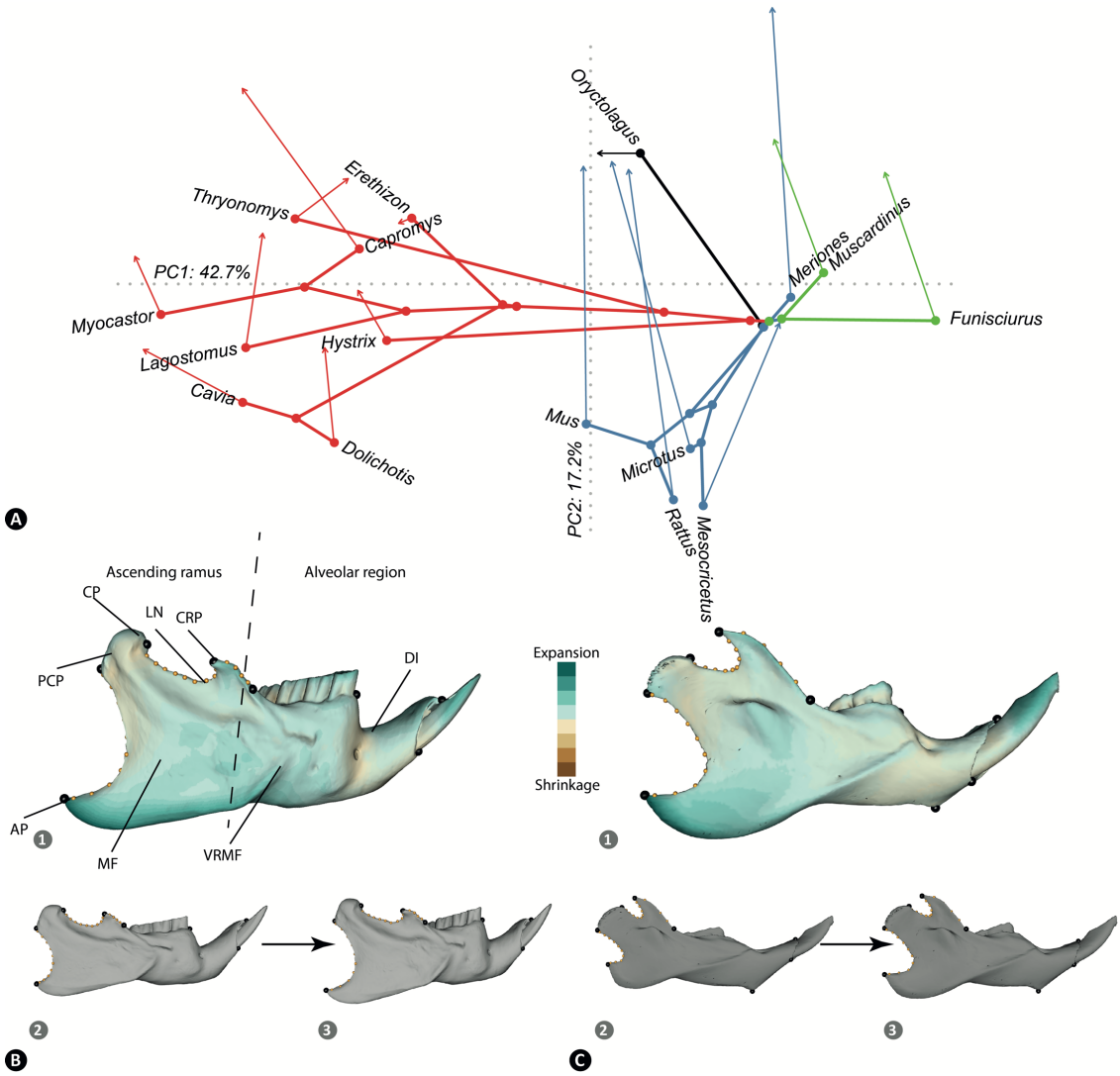

Figure 3. Developmental morphospace and shape changes associated with the phylogenetic mean postnatal trajectory. A. Developmental morphospace where average juveniles of species are represented as the tip of the phylogenetic branches, postnatal trajectories are represented as arrows from the juvenile to adult shapes. Red is for Hystricomorpha species, blue for Myomorpha species, green for Sciuromorpha species and black for Lagomorpha; B: Shape changes associated with the phylogenetic mean postnatal trajectory mapped on the Hystricomorpha mean shape (AP: angular process, CP: condylar process, DI: diastema, CRP: coronoid process, LN: lunar notch, MF: masseter fossa, PCP: postcondylar process, VRMF: ventral ridge of masseter fossa); C: Shape changes associated with the phylogenetic mean postnatal trajectory mapped on the Myomorpha mean shape. Green areas represent expansion from juvenile to adult shapes, whereas beige areas correspond to a compression effect. Gray shapes correspond to the juvenile mean shape (2) or to the modeling of adult mean shape (3) according to the juvenile mean shape plus the phylogenetic mean trajectory $\bar{\boldsymbol{z}}_{pgls}$. See also Movie S1 for dynamic shape changes.

Variation is concentrated on the first two PCs, which account for 59,9% of the total shape variance (Fig. 3A), with 90% for the first eight PCs. Myomorpha and Hystricomorpha are opposed on PC1, which accounts for 42,7% of shape variance. This pattern is expected, since mandible anatomy differs strongly between the two suborders. Developmental vectors (the arrows in Fig. 3A) appear to be mainly orthogonal to this shape divergence and project consistently on PC2. In this 2D projection,

these postnatal trajectories in Myomorpha appear to be oriented in similar directions, while the vectors of Hystricomorpha seem less consistent with this general trend. Sciuromorpha are placed close to Myomorpha and their developmental vectors seem to follow the same main direction. The special case of *Muscardinus*, which has a myomorphous skull structure but belongs to the Sciuromorpha suborder, does not seem to be more similar to the trajectories of Myomorpha species.

The PC2 axis seems to summarize a growth trajectory common among rodents. The phylogenetic mean of postnatal shape trajectory $\bar{\boldsymbol{z}}_{pgls}$, which corresponds to the ancestral pattern of postnatal shape changes, is in close agreement with the shape changes described by PC2 (α = 41.4°, p < 0.0001). Suborder estimates $\hat{\boldsymbol{z}}$ of the postnatal trajectory are at 31.1° $\pm$ 7.2 of this common growth pattern described along PC2 for Myomorpha, at 58.9° $\pm$ 14.9 for Hystricomorpha, and at 49.6° $\pm$ 6.6 for Sciuromorpha. These angles are more similar than expected between two random directions (p < 0.0001). On average, 47.3% $\pm$ 0.22 of these vectors map onto PC2, with the remainder spread over all the other PCs. The estimation of the postnatal vectors and derived parameters seem robust given the amount of change and species differences to the number of sampled juveniles (Fig. S1). They may also be sensitive to variation in age of juveniles because of the non-linearity of postnatal trajectories (Sheets and Zelditch 2013). Nonetheless, the vectors are still describing a roughly similar direction in the shape space and for instance differences in angles with $\bar{\boldsymbol{z}}_{pgls}$ due to age variation are smaller than the observed angles (Table S2).

Postnatal shape changes described by the ancestral pattern of growth $\bar{\boldsymbol{z}}_{pgls}$ (Fig. 3BC; Movie S1) imply elongation of the condylar and postcondylar processes, with strong bending of the lunar notch. The angular process expands and subsides while the anterior part of the ventral ridge of the ramus retreats, increasing the ramus. The diastema elongates and flattens. The alveolar region is proportionally larger in the juvenile mandible, whereas in the adult mandible the alveolar region is of similar proportions to the ascending ramus.

The apparent orthogonality observed between the phylogenetic signal and the postnatal development on the first PCs of the developmental morphospace is actually weaker than supposed from the preceding. Whereas the first phylogeny-aligned component is clearly orthogonal to $\bar{\boldsymbol{z}}_{pgls}$ or to the suborder estimates $\hat{\boldsymbol{z}}$, additional phylogeny-aligned components are more similar to some of these trajectories, implying that some divergences may have happen along similar directions than the postnatal development (Fig. 4A). The overall angle with the Hystricomorpha estimate $\hat{\boldsymbol{z}}$ is larger (Fig. 4A) and it could be noted the striking difference between suborder estimates on the second component (Fig. 4B). These results suggest that the divergences in this suborder are somehow less related to its main pattern of postnatal changes. The overall congruence between evolutionary divergences and developmental directions is even stronger. Krzanowski's common subspace analysis shows that species divergences share some shape changes with the main patterns of postnatal changes. The first five eigenvalues $\boldsymbol{\Delta}$ of **H** range between 1.67 and 1.96 (for a maximum of 2) and the individual angles $\boldsymbol{\delta}$ between the eigenvectors of **H** and the postnatal or evolutionary matrices ranges from 7.7° and 23.9°.

Levels of adult and juvenile disparities

Given the levels of agreement between evolutionary changes and growth directions, an increase in disparity between juveniles and adults could be expected. However, such an increase is observed only in Myomorpha and is only marginal (Fig 4A, Table S3). On contrary in Hystricomorpha, disparity seems to be established in the early stages, as levels of disparity are similar in juveniles and in adults. Disparity in Myomorpha juveniles accumulates more slowly than for the other three clade × age groups (Fig. 4B). In particular, disparity based on the main patterns of differentiation between species and developmental stages (the first PCs) is much lower in juvenile than in adult Myomorpha,

a pattern that is not observed in Hystricomorpha. This suggests that Myomorpha juveniles have a relatively undifferentiated mandible among species, given the broad pattern of differentiation of the mandible observed at the scale of the order.

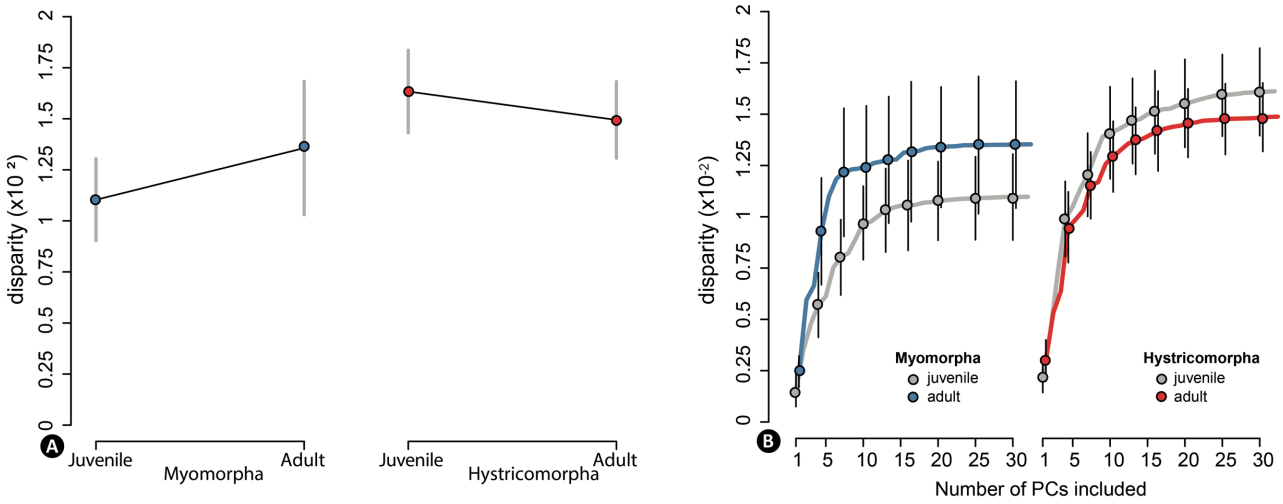

Figure 4. Developmental changes in disparity. A. Comparison of levels of disparity between juveniles and adults within suborders. B. Accumulation curves of juvenile and adult disparities along the principal components of the developmental morphospace. Blue is for Myomorpha and red is for Hystricomorpha.

Evolution of postnatal shape changes

The observed variation in postnatal shape trajectories (the arrows in Figure 3) appears consistent with a phylogenetic signal (Fig. 5A-C). Species trajectories cluster within suborders both in direction and magnitude. The main pattern of changes shows an opposition between larger postnatal shape changes on negative values of PC1 and smaller ones on positive values (Fig. 5B). These variations agree with a pattern expected under Brownian divergence (K_{mult} = 0.42, p = 0.04), as was the case for the spreading of species in the developmental morphospace for both adults (K_{mult} = 0.91, $p < 1 \times 10^{-4}$) and juveniles (K_{mult} = 0.93, $p < 1 \times 10^{-4}$). However, the effect size is much smaller for developmental trajectory than for shape (Z = 1.78 versus 4.60 for adults and 4.96 for juveniles), suggesting a less neutral divergence and species-specific postnatal growth trajectories.

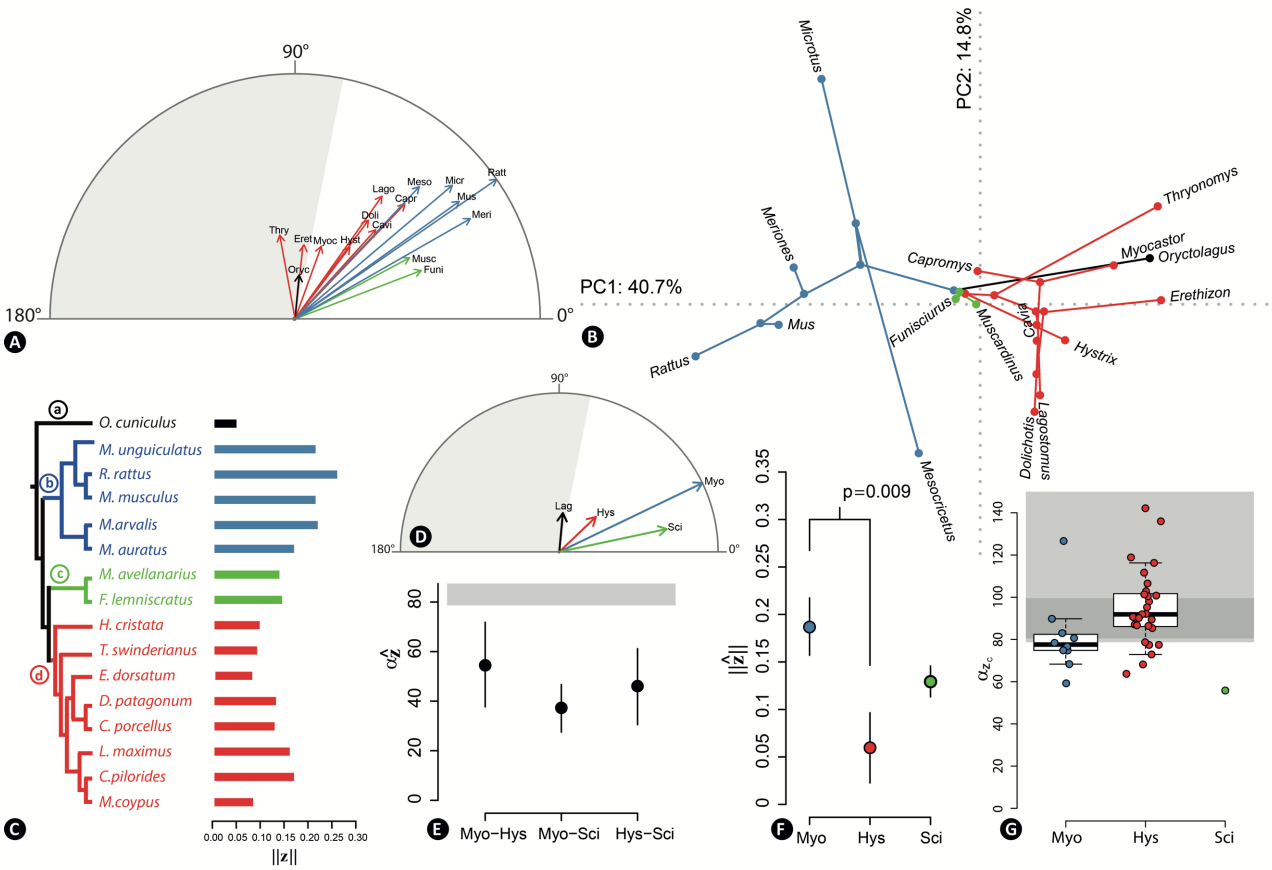

Figure 5. Variation of postnatal trajectories. A. Angles between the postnatal trajectories of species ($\boldsymbol{z}$) and the phylogenetic mean ($\bar{\boldsymbol{z}}_{pgls}$). The lengths of the vectors are proportional to their norm; B. The principal component ordination of the postnatal trajectories ($\boldsymbol{z}$) together with the projection of the phylogeny; C. Magnitude of postnatal shape changes; D. Angles between the estimates of suborder trajectories ($\hat{\boldsymbol{z}}$) and the common growth pattern $\bar{\boldsymbol{z}}_{pgls}$; E. Angles between the estimates of suborder trajectories ($\hat{\boldsymbol{z}}$); F. Magnitude of the suborder estimates of postnatal changes; G**.** Angles between $\boldsymbol{z}_c$ within suborders Gray shading in panel A, D, E corresponds to the distribution of angles between random vectors with a probability > 0.05. See Figure 3 for color scheme and species acronyms.

In agreement with this phylogenetic signal, the suborder trajectories $\hat{\boldsymbol{z}}$ of agree with the common growth pattern (Fig. 5D). The deviation between these suborder estimates (Fig. 5E) is 54.7° ± 17.4° (Myomorpha vs Hystricomorpha), 37.1° ± 9.4° (Myomorpha vs Sciuromorpha), and 45.8° ± 15.1° (Hystricomorpha vs Sciuromorpha). These angles are more similar than expected between two random directions ($p < 0.0001$). These elements support a relative conservation of the main pattern of postnatal changes of the mandible in rodents. However, the magnitude of postnatal shape changes $\|\hat{\boldsymbol{z}}\|$ differs between Myomorpha and Hystricomorpha ($t_{12} = 2.70$, $p = 0.009$), with larger vectors in the latter (Fig. 5F).

Once removed the expected patterns under Brownian divergence, the approximately phylogeny-corrected trajectories $\boldsymbol{z}_c$ still present important variation within and among suborders (Fig 5G). These angles between phylogeny-corrected vectors $\boldsymbol{z}_c$ are large, indicating species specificities and divergence of individual trajectories. For many species comparisons, this angle is still more similar than expected for random vectors. This evidences a relative conservation of the ancestral main pattern of growth.

To assess the influence of life history traits and tooth growth on this remaining variation in trajectories, a phylogenetic generalized least-squares was performed. Gestation time and duration of pre-weaning period were pooled within suborders prior to analysis as they present a very high correlation with deep node in the phylogeny (Fig. 1). It appears that only type of tooth growth has an effect after controlling for Brownian expectation of evolutionary divergence (Table 1).

Table **1**. Phylogenetic generalized least-squares of postnatal trajectories.

Source	Df	SS	MS	r^2	F	Z	Pr(>F)
Gestation length	1	0.02228	0.022283	0.05460	1.0948	0.37464	0.3675
Weaning age	1	0.03433	0.034328	0.08411	1.6866	1.10556	0.1411
Litter per year	1	0.02846	0.028462	0.06974	1.3984	0.79606	0.2203
Tooth growth	2	0.08831	0.044156	0.21639	2.1695	1.94286	0.0252
Residuals	10	0.20353	0.20353	0.49871			

Simulations show that appropriate type-I error is returned and adequate power could be obtained for large effects (Table S4 and Fig. S2). Pairwise comparisons between types of tooth growth show that hypselodonty has a different effect from brachyodonty (d = 0.132 Z = 3.36, p = 0.002) and hypsodonty (d = 0.117, Z = 1.83, p = 0.05), whereas the effect of brachyodonty is similar to that of hypsodonty (d = 0.087, Z = 0.934, p = 0.17).

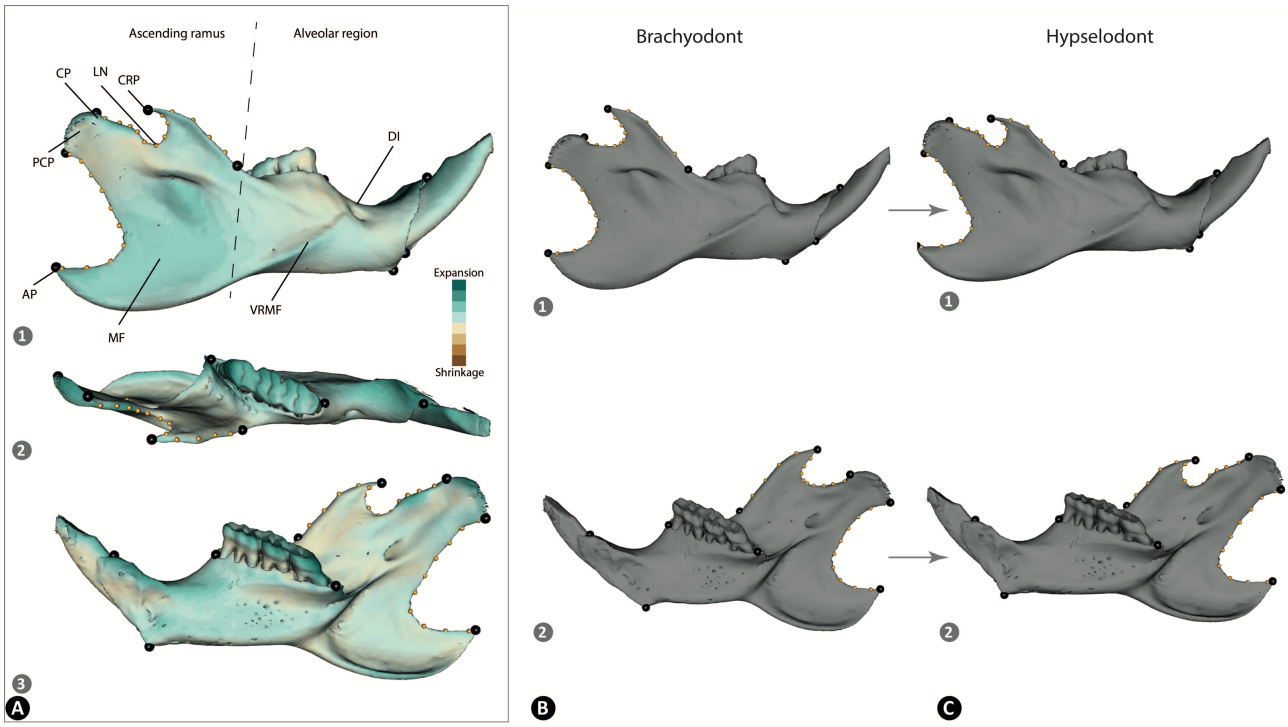

Figure 6. Shape changes associated with dental growth: brachyodont versus hypselondont. Effects are mapped on the mean shape of myomorph specimens. Green areas represent expansion from brachyodont to hypselodont shapes, whereas beige areas correspond to a compression effect. See also Movie S2 for dynamic shape changes. (AP: angular process, CP: condylar process, DI: diastema, CRP: coronoid process, LN: lunar notch, MF: masseter fossa, PCP: postcondylar process, VRMF: ventral ridge of masseter fossa). 1: labial view; 2: upper view; 3: lingual view. Gray shapes correspond

to the least square estimates of the B: brachyodont or C: hyselodont shapes. 1: labial view; 2: lingual view.

Shape changes in relation to hypselodonty (Fig. 6 and Movie S2) show an extension of the condylar process, which rises vertically and becomes thinner, and a thicker diastema, especially in its upper part. The molar area increases in volume, as does the anterior part of the ventral ridge of the masseter fossa. The alveolar region is more robust and extends further on the lingual side.

Discussion

Conservation of the main patterns of growth and evolutionary divergences

Our main results highlight a general pattern of shape changes during postnatal development across Rodentia, with similar local bone growth. The mandible shape in juveniles is generally elongated and flattened, with relatively short processes. These processes later expand, increasing their relative height and thus enlarging the masseter fossa. This ontogenetic modification of the posterior part of the mandible, well described in laboratory mice (Swiderski and Zelditch 2013), and observed in Sciuridae (Zeldtich et al. 2016), is here shown to be conserved across the main clades of Rodentia. This pattern is undoubtedly related to the development of the muscular complex inserting on the mandible. As these muscles gain volume during growth, their contact surface with the bone must expand. Similarly, the different processes become more robust after weaning to support the attachment tension of the muscles. This musculoskeletal system articulates with the skull (cranium and mandible) to allow mastication, which will impose greater mechanical constraints at this life stage (Scott et al. 2014). This general pattern of growth appears orthogonal to the main shape divergence between suborders, which opposes the mandible shape of Hystricomorpha with the ones of Myomorpha and Sciuromorpha. This contrast corresponds to gross differences in anatomy, the mandibular structure of Tullberg (1899), opposing hystricognaths and sciurognaths based on the opposite orientation of the angular and condyloid processes.

Evolutionary divergences between species appear nonetheless much more related to the ontogenesis and its variation than expected from the orthogonality of their main directions, suggesting that developmental processes such as heterochrony could have played a role in species divergences. Based on the sampled species, Hystricomorpha exhibit developmental patterns that are much more genus-specific than those of Myomorpha species, where the trajectories are more similar to the common developmental pattern. This difference seems to be mainly related to the difference in species divergence between suborders. Myomorpha have a common juvenile shape that diverges postnatally among sub-families. In Hystricomorpha, beside the common juvenile pattern, the mandible shape of juveniles presents some species-specific features from the early stages, and the magnitude of postnatal shape changes is smaller. Hystricomorpha being not precisely age controlled and in smaller numbers compared to Myomorpha, variation observed in Hystricomorpha could be more biased by some age or sampling effects (Fig S1 and Table S2). These biases may partly explain some variation observed between the suborders. Nonetheless, the differences between suborders could also be explained by the vast differences between the ecological traits for each suborder (Wolff and Sherman 2009), including reproductive strategy, gestation, and weaning (acting directly on pup development), diet (leading to more or less mechanical stress on the masticatory apparatus), and taxonomic richness (reflecting the diversity of a clade). Myomorpha newborns share common anatomical features, whereas the longer gestational period in Hystricomorpha allows longer in-utero development, producing a skeletonized and differentiated organ (Huggett and Widdas 1951). In this respect, the peculiarity of gerbils (*Meriones*) is revealing as this species has a longer gestation than

other Myomorpha species and presents at seven days old a more differentiated juvenile mandible as the Hystricomorpha species.

This developmental difference between Myomorpha and Hystricomorpha suggests that juvenile disparity at birth is partly driven by timing differences in the skeletonization and differentiation processes in relation to variation in gestational duration. Therefore, the potential for plasticity after birth is likely to be different between the two suborders since the mandible at birth is not at the same state of ossification and differentiation.

Evolution of postnatal trajectories

Variation in gestational length may explain changes in postnatal trajectories because it modifies the onset of the postnatal period. It could thus explain variation in magnitude of postnatal changes as juveniles could be more or less differentiated and skeletonized at birth. The observed differences in magnitude between suborders could be related to such factor. As developmental trajectories are strongly non-linear (Green et al. 2017), variation in the onset of postnatal growth will affect the linear approximation of the postnatal trajectory leading to variation in angles in relation to differential duration of the gestation. Again, variation between suborders seems to be related to such an effect. However, once the expected effect of Brownian divergence was factored in, no effect of the gestational duration was observed to explain the residual differences in postnatal shape changes. The separation between suborders is ancient and occurred during the Paleocene (Swanson et al., 2019). Deep-rooted phylogenic signal strongly structures traits and aggregates them, as gestational length or weaning timing, within clades. These correlations potentially mask differences related to ecological traits.

The weaning period and dietary diversification occurring within this period could also play a role in the divergences of postnatal trajectories as different behaviors and feeding habits lead rodents to adapt their chewing movement. Rodents can gnaw with their incisors as well as chew with their cheek-teeth (Byrd 1981, Cox et al. 2012, Hiiemäe and Ardran 1968). These movements, acquired more or less rapidly during weaning, could induce new mechanical constraints and thus change the pattern of bone remodeling (Jacobs 1984). Changes in the consistency of food are known to induce plasticity of the mandible, with a large effect on the angular and coronoid processes, modifying the correlation between the alveolar and muscle-bearing regions and their biomechanics (Anderson et al. 2014). In Myomorpha species, weaning is rapid and therefore mechanically brutal (Curley et al. 2009). This rapid upheaval in diet could explain the major changes observed in morphology. The feeding system must change from the sucking movement to active chewing in only a few days. In mice, bite force increases drastically in the days preceding weaning (Ginot et al. 2020). In the Hystricomorpha species, parental care is different, with long behavioral weaning and less brutal dietary weaning, over a much longer period (Wolff and Sherman 2008). As the Hystricomorpha species, at least the ones sampled in this study, are born with a more differentiated shape and present postnatal shape changes of smaller magnitude during a longer period, dietary changes at weaning have likely less impact on the patterns of correlated bone remodeling. Guinea pigs (*Cavia*) have a short weaning timing of 18 days comparable to the one of the Myomorpha species but present nonetheless a magnitude and direction of postnatal trajectory similar to other Hystricomorpha species. As with gestation, no effect of the weaning period was observed to explain the residual differences in postnatal shape changes once the expected effect of Brownian divergence was factored in, but again weaning period timing is strongly aggregated within each clade.

Only tooth growth, especially molar hypselodonty, appears to produce a special signature on the postnatal shape changes of the mandible. Within Myomorpha, hypselodonty in arvicolines may explain the divergence of their postnatal trajectory, as their unrooted prismatic teeth strongly modify

the dental alveolar region. A comparable effect of tooth growth has been shown on individual postnatal ontogenies in mice (Swiderski and Zelditch 2013). During development, bone and teeth interact with each other and these interactions may explain important changes either in bone or in tooth. For instance, tooth-bone mechanical interaction explains the lateral offset of molar cusps during development, a repeated evolutionary innovation in the mammalian tooth pattern (Renvoisé et al. 2017). This interaction influences also the mandible shape as it is modified with arrested tooth development in mutant mice (Paradis et al. 2013, Boughner et al. 2018). Thus, the bone must adapt to the dynamic process of tooth growth, which imposes new biomechanical stresses. This dynamic reconfiguration of bone strain imposes a new spatialization of bone formation and remodeling (Martinez-Vargas et al. 2017), that may have evolutionary outcomes in both tooth and bone shapes.

Our results suggest that evolutionary changes in the postnatal development of the mandible could be related to muscle and tooth development. The mandible responds dynamically to both the growth of the dental alveoli and the development of the masticatory muscles (Swiderski and Zelditch 2013). The biomechanics of mastication functionally integrates the alveolar and ramus regions from their direct epigenetic interactions (Zelditch et al. 2008). Changes in environment (e.g., diet or behavior) could induce changes in the spatialization of biomechanical strain and therefore of bone remodeling, because of the intricate relationship between the mandible and tooth and muscle growth. If tooth or muscle growth drives mandible plasticity, natural selection on these anatomical elements will induce correlated changes in the mandible via epigenetic interactions, which may in turn be subject to genetic accommodation (West-Eberhard 2003, Uller et al. 2020). For example, at a smaller scale, the repeated dietary adaptation in mice observed following their invasion of sub-Antarctic islands seems to agree with a similar scenario, with mandible plasticity as the main process at the early stages of the invasion (Renaud et al. 2018).

Comparison with the cranium

Despite a common pattern of postnatal changes in relation to muscle and tooth growth, mandibles are quite different between suborders suggesting that ontogeny did not constrained anatomical diversity. At its highest level (hystricognaths versus sciurognaths), this diversity occurs mainly in an orthogonal direction of the common postnatal growth pattern. This independence of anatomical diversity to developmental constraints was similarly observed for the cranium (Wilson 2013, Wilson and Sanchez-Villaga 2010). However, at a lower scale, the diversity of postnatal trajectories (i.e. variation in the magnitude of changes and angles) appears to be specific to the suborders. This observation contrasts with the constrained variation of allometric patterns observed on the cranium (Wilson 2013, Wilson and Sanchez-Villaga 2010). Within the head, the cranium is a composite unit composed of multiple bones, and this assemblage is constrained by the development of teeth (Renaud et al. 2009), facial muscles (Ravosa et al. 2008), and internal organs (i.e. the brain, Richtsmeier and Flaherty 2013, or the olfactory and auditory organs, Barone 1976). This complexity may explain the low skull disparity in relation to lineage diversification described in Rodentia (Alhajeri and Steppan 2018), or in the adaptive radiation of some families (Maestri et al. 2017), or the relatively overlapping growth pattern of the skull observed among rodent clades (Wilson 2013). The higher complexity of skull development is thought to reduce its dependence on muscle and tooth development (Swiderski and Zelditch 2013), and this difference in complexity probably explains the contrast observed between these two skeleton elements of the head.

Conclusion

In conclusion, the main evolutionary and developmental patterns appear to be along orthogonal directions of the shape space. Beside these main patterns, most of the shape divergences

arise along postnatal directions of growth. The filling of the morphospace varies between rodent suborders being mainly during the gestational period in Hystricomorpha and during the postnatal growth in Myomorpha. The postnatal trajectories of Myomorpha subfamilies are closer, but present a much stronger magnitude of changes over a shorter growth period. Among Hystricomorpha, part of the observed adult shape is set up prenatally, and most postnatal trajectories are genus-specific, which agrees with non-linear developmental trajectories over longer gestational periods. Juvenile mandibles present similarities among suborders, with a flattened shape. Mandible shape then diversifies during growth in relation to muscle and tooth development, with epigenetic interactions coordinating the changes in the alveolar and muscle-bearing regions. This functional integration by biomechanical interactions might have favored evolutionary changes driven by developmental plasticity, but the importance of this process is likely to differ between rodent suborders.

Data availability

The landmark data that supports the findings of this study are available on Dryad.

References

Adams, D. (2014). A Generalized K statistic for estimating phylogenetic signal from shape and other high-dimensional multivariate data. Systematic Biology, 63, 685-697.

Adams, D. C., Collyer, M., Kaliontzopoulou, A., & Sherratt, E. (2016). geomorph: Software for geometric morphometric analyses. R Package.

Adams, D. C., & Collyer, M. L. (2018). Multivariate phylogenetic comparative methods: Evaluations, comparisons, and recommendations. Systematic Biology, 67, 14–31.

Agostinelli, C., & Lund, U. (2017). R package 'circular': Circular Statistics. R Package.

Alberch, P. (1980). Ontogenesis and morphological diversification. American Zoologist, 20, 653–667.

Alberch, P. (1982). Developmental constraints in evolutionary processes. In Evolution and development (pp. 313-332). Springer, Berlin, Heidelberg.

Alberch, P., Gould, S. J., Oster, G. F., & Wake, D. B. (1979). Size and shape in ontogeny and phylogeny. Paleobiology, 296-317.

Alhajeri, B. H., & Steppan, S. J. (2018). Disparity and evolutionary rate do not explain diversity patterns in Muroid rodents (Rodentia: Muroidea). Evolutionary Biology, 45, 324–344.

Álvarez, A., & Pérez, M. E. (2019). Deep changes in masticatory patterns and masseteric musculature configurations accompanied the eco-morphological evolution of cavioid rodents (Hystricognathi, Caviomorpha). Mammalian Biology, 96, 53–60.

Anderson, P. S., Renaud, S., & Rayfield, E. J. (2014). Adaptive plasticity in the mouse mandible. BMC Evolutionary Biology, 14, 85.

Arnold, S. F. (1981). The theory of linear models and multivariate analysis. John Wiley & Sons, Inc. New York.

Arthur, W. (2001). Developmental drive: an important determinant of the direction of phenotypic evolution. Evolution & development, 3(4), 271-278.

Atchley, W. R. (1993). Genetic and developmental aspects of variability in the mammalian mandible. The Skull, 1, 207–247.

Barone, R. (1976). Anatomie comparée des mammifères domestiques. Tome 1: ostéologie, 2ème édition. Paris: ed. Vigot Frères.

Bookstein, F. L. (2016). The inappropriate symmetries of multivariate statistical analysis in geometric morphometrics. Evolutionary Biology, 43, 277–313.

Boughner, J. C., Eede, M. C. van, Spring, S., Yu, L. X., Rostampour, N., & Henkelman, R. M. (2018). P63 expression plays a role in developmental rate, embryo size, and local morphogenesis.

Developmental Dynamics, 247, 779–787.
Brandt, J. F. (1855). Beiträge zur nähern Kenntniss der Säugethiere Russland's (Vol. 7). Kaiserl. Academ. d. Wiss.
Byrd, K. E. (1981). Mandibular movement and muscle activity during mastication in the guinea pig (*Cavia porcellus*). Journal of Morphology, 170, 147–169.
Cardini, A., & Thorington Jr, R. W. (2006). Postnatal ontogeny of marmot (Rodentia, Sciuridae) crania: allometric trajectories and species divergence. Journal of Mammalogy, 87(2), 201-215.
Collyer, M. L., & Adams, D. C. (2018). RRPP: An r package for fitting linear models to high-dimensional data using residual randomization. Methods in Ecology and Evolution, 9, 1772–1779.
Collyer, M. L., & Adams, D. C. (2020). Phylogenetically aligned component analysis. Methods in Ecology and Evolution.
Cox, P. G., & Hautier, L. (2015). Evolution of the Rodents: Advances in Phylogeny, Functional Morphology and Development. Cambridge University Press.
Cox, P. G., Rayfield, E. J., Fagan, M. J., Herrel, A., Pataky, T. C., & Jeffery, N. (2012). Functional Evolution of the Feeding System in Rodents. PLOS ONE, 7, e36299.
Curley, J. P., Jordan, E. R., Swaney, W. T., Izraelit, A., Kammel, S., & Champagne, F. A. (2009). The Meaning of weaning: influence of the weaning period on behavioral development in mice. Developmental Neuroscience, 31, 318–331.
Darwin, C. (1859). On the origin of species. John Murray, London.
Dibner, J. J., Richards, J. D., Kitchell, M. L., & Quiroz, M. A. (2007). Metabolic challenges and early bone development. Journal of Applied Poultry Research, 16, 126–137.
Drake, A. G., & Klingenberg, C. P. (2010). Large-scale diversification of skull shape in domestic dogs: Disparity and modularity. The American Naturalist, 175, 289–301.
Eble, G. J., Crutchfield, J. P., & Schuster, P. (2003). Evolutionary dynamics: exploring the interplay of selection, accident, neutrality, and function. Oxford University Press.
Efron, B. (1979). Bootstrap Methods: Another Look at the Jackknife. The Annals of Statistics, 7, 1-26.
Erwin, D. H. (2007). Disparity: morphological pattern and developmental context. Palaeontology, 50, 57–73.
Foote, M. (1994). Morphological disparity in Ordovician-Devonian crinoids and the early saturation of morphological space. Paleobiology, 20, 320–344.
Fusco, G. (2008). Evolving Pathways: Key themes in evolutionary developmental biology. Cambridge University Press.
Gerber, S. (2014). Not all roads can be taken: development induces anisotropic accessibility in morphospace. Evolution & Development, 16, 373–381.
Ginot, S., Hautier, L., Agret, S., & Claude, J. (2020). Decoupled ontogeny of in vivo bite force and mandible morphology reveals effects of weaning and sexual maturation in mice. Biological Journal of the Linnean Society, 129(3), 558-569.
Gould, S. J. (1977). Ontogeny and Phylogeny. Harvard University Press.
Green, R. M., Fish, J. L., Young, N. M., Smith, F. J., Roberts, B., Dolan, K., Choi, I., each, C. L., Gordon, P., Cheverud, J. M., Roseman, C. C., Williams, T. J., Marcucio, R. S. & Hallgrímsson, B. (2017). Developmental nonlinearity drives phenotypic robustness. Nature communications, 8(1), 1-12.
Gunz, P., Mitteroecker, P., & Bookstein, F. L. (2005). Semilandmarks in three dimensions. In D. E. Slice (Ed.), Modern Morphometrics in Physical Anthropology (pp. 73–98). Springer US.
Hallgrímsson, B., Brown, J. J., Ford-Hutchinson, A. F., Sheets, H. D., Zelditch, M. L., & Jirik, F. R. (2006). The brachymorph mouse and the developmental-genetic basis for canalization and morphological integration. Evolution & development, 8(1), 61-73.

Hallgrímsson, B., & Hall, B. K. (Eds.). (2011). Epigenetics: linking genotype and phenotype in development and evolution. University of California Press.

Hautier, L. (2010). Masticatory muscle architecture in the gundi *Ctenodactylus vali* (Mammalia, Rodentia). Mammalia, 74, 153–162.

Hautier, L., Michaux, J., Marivaux, L., & Vianney-Liaud, M. (2008). Evolution of the zygomasseteric construction in Rodentia, as revealed by a geometric morphometric analysis of the mandible of Graphiurus (Rodentia, Gliridae). Zoological Journal of the Linnean Society, 154(4), 807–821.

Herring, S. W. (2011). Muscle-bone interactions and the development of skeletal phenotype: jaw muscles and the skull. In Hallgrímsson, B., & Hall, B. K. (Eds), Epigenetics: Linking Genotype and Phenotype in Development and Evolution. University of California Press, 221-237.

Hiiemäe, K. M., & Ardran, G. M. (1968). A cinefluorographic study of mandibular movement during feeding in the rat (*Rattus norvegicus*). Journal of Zoology, 154, 139–154.

Houle, D., & Meyer, K. (2015). Estimating sampling error of evolutionary statistics based on genetic covariance matrices using maximum likelihood. Journal of Evolutionary Biology, 28(8), 1542-1549.

Huggett, A. S. G., & Widdas, W. F. (1951). The relationship between mammalian foetal weight and conception age. The Journal of Physiology, 114, 306–317.

Jacobs, L. L. (1984). Rodentia: Extraordinary diversification of a morphologically distinctive and stereotyped order. Series in Geology, Notes for Short Course, 8, 155–166.

Kavanagh, K. D., Shoval, O., Winslow, B. B., Alon, U., Leary, B. P., Kan, A., & Tabin, C. J. (2013). Developmental bias in the evolution of phalanges. Proceedings of the National Academy of Sciences, 110(45), 18190-18195.

Klingenberg, C. P. (1998). Heterochrony and allometry: the analysis of evolutionary change in ontogeny. Biological Reviews, 73, 79–123.

Klingenberg, C. P. (2020). Walking on Kendall's Shape Space: Understanding Shape Spaces and Their Coordinate Systems. Evolutionary Biology, 47, 334–352.

Klingenberg, C. P., & Navarro, N. (2012). Development of the mouse mandible: a model system for complex morphological structures. Evolution of the house mouse, 135, 149.

Krzanowski, W. J. (1979). Between-groups comparison of principal components. Journal of the American Statistical Association, 74(367), 703-707.

Laffont, R., & Navarro, N. (2019). Digitalization of 3D landmarks on mesh. R Package.

Li, S. (2011). Concise formulas for the area and volume of a hyperspherical cap. Asian Journal of Mathematics and Statistics, 4, 66–70.

Lieberman, D. E. (2011). Epigenetic integration, complexity, and evolvability of the head: rethinking the functional matrix hypothesis. In Hallgrímsson, B., & Hall, B. K. (Eds), Epigenetics: Linking Genotype and Phenotype in Development and Evolution, 271–289.

Maestri, R., Monteiro, L. R., Fornel, R., Upham, N. S., Patterson, B. D., & Freitas, T. R. O. de. (2017). The ecology of a continental evolutionary radiation: Is the radiation of sigmodontine rodents adaptive? Evolution, 71, 610–632.

Magalhães, J. P. D., & Costa, J. (2009). A database of vertebrate longevity records and their relation to other life-history traits. Journal of Evolutionary Biology, 22, 1770–1774.

Marcus, L., & Hingst-Zaher, E. (2000). Application of landmark morphometrics to skulls representing the orders of living mammals. Hystrix, the Italian Journal of Mammalogy, 11, 27-47.

Martinez-Maza, C., Freidline, S. E., Strauss, A., & Nieto-Diaz, M. (2016). Bone growth dynamics of the facial skeleton and mandible in Gorilla gorilla and Pan troglodytes. Evolutionary Biology, 43(1), 60-80.

Martínez-Vargas, J., Muñoz-Muñoz, F., Martinez-Maza, C., Molinero, A., & Ventura, J. (2017).

Postnatal mandible growth in wild and laboratory mice: Differences revealed from bone remodeling patterns and geometric morphometrics. Journal of Morphology, 278, 1058–1074.
Menegaz, R. A., & Ravosa, M. J. (2017). Ontogenetic and functional modularity in the rodent mandible. Zoology, 124, 61–72.
Meyer, K., & Houle, D. (2013, October). Sampling based approximation of confidence intervals for functions of genetic covariance matrices. In Proc. Assoc. Advmt. Anim. Breed. Genet (Vol. 20, pp. 523-526).
Mitteroecker, P., & Bookstein, F. (2009). The Ontogenetic trajectory of the phenotypic covariance matrix, with examples from craniofacial shape in rats and humans. Evolution, 63, 727–737.
Navarro, N. (2003). MDA: a MATLAB-based program for morphospace-disparity analysis. Computers & Geosciences, 29, 655–664.
Nijhout, H. F., & Emlen, D. J. (1998). Competition among body parts in the development and evolution of insect morphology. Proceedings of the National Academy of Sciences, 95, 3685–3689.
Nowak, R. M., & Walker, E. P. (1999). Walker's Mammals of the World (Vol. 1). JHU press.
Olsen, B. R., Reginato, A. M., & Wang, W. (2000). Bone development. Annual Review of Cell and Developmental Biology, 16, 191–220.
Paradis, E., & Schliep, K. (2019). ape 5.0: an environment for modern phylogenetics and evolutionary analyses in R. Bioinformatics, 35, 526–528.
Paradis, M. R., Raj, M. T., & Boughner, J. C. (2013). Jaw growth in the absence of teeth: the developmental morphology of edentulous mandibles using the p63 mouse mutant. Evolution & development, 15(4), 268-279.
Ravosa, M. J., López, E. K., Menegaz, R. A., Stock, S. R., Stack, M. S., & Hamrick, M. W. (2008). Using “Mighty Mouse” to understand masticatory plasticity: myostatin-deficient mice and musculoskeletal function. Integrative and Comparative Biology, 48, 345–359.
Renaud, S., Auffray, J.-C., & de la Porte, S. (2010). Epigenetic effects on the mouse mandible: common features and discrepancies in remodeling due to muscular dystrophy and response to food consistency. BMC Evolutionary Biology, 10, 28.
Renaud, S., Ledevin, R., Pisanu, B., Chapuis, J. L., Quillfeldt, P., & Hardouin, E. A. (2018). Divergent in shape and convergent in function: Adaptive evolution of the mandible in Sub-Antarctic mice. Evolution, 72(4), 878-892.
Renaud, S., Pantalacci, S., Quéré, J.-P., Laudet, V., & Auffray, J.-C. (2009). Developmental constraints revealed by co-variation within and among molar rows in two murine rodents. Evolution & Development, 11, 590–602.
Renvoisé, E., Kavanagh, K. D., Lazzari, V., Häkkinen, T. J., Rice, R., Pantalacci, S., Salazar-Ciudad, I., & Jernvall, J. (2017). Mechanical constraint from growing jaw facilitates mammalian dental diversity. Proceedings of the National Academy of Sciences, 114, 9403–9408.
Renvoisé, E., & Montuire, S. (2015). Developmental mechanisms in the evolution of phenotypic traits in rodent teeth. In P. G. C. & L. Hautier (Ed.), Evolution of the Rodents: advances in phylogeny, functional morphology and development, 478–509. Cambridge University Press.
Revell, L. J. (2009). Size-correction and principal components for interspecific comparative studies. Evolution: International Journal of Organic Evolution, 63(12), 3258-3268.
Revell, L. J. (2012). phytools: an R package for phylogenetic comparative biology (and other things): phytools: R package. Methods in Ecology and Evolution, 3, 217–223.
Richtsmeier, J. T., & Flaherty, K. (2013). Hand in glove: brain and skull in development and dysmorphogenesis. Acta Neuropathologica, 125, 469–489.
Rohlf, F. J. (2001). Comparative methods for the analysis of continuous variables: geometric interpretations. Evolution, 55(11), 2143-2160.

Rohlf, F. J., & Corti, M. (2000). Use of two-block partial least-squares to study covariation in shape. Systematic Biology, 49, 740–753.

Salazar-Ciudad, I. (2021). Why call it developmental bias when it is just development?. Biology Direct, 16, 1-13.

Schabenberger, O., & Gotway, C. A. (2017). Statistical methods for spatial data analysis. CRC Press.

Schlager, S. (2017). Chapter 9 - Morpho and Rvcg – Shape analysis in R: R-Packages for geometric morphometrics, shape analysis and surface manipulations. In G. Zheng, S. Li, & G. Székely (Eds.), Statistical Shape and Deformation Analysis, 217–256. Academic Press.

Scott, J. E., McAbee, K. R., Eastman, M. M., & Ravosa, M. J. (2014). Teaching an old jaw new tricks: diet-induced plasticity in a model organism from weaning to adulthood. Journal of Experimental Biology, 217, 4099–4107.

Sheets, H. D., & Zelditch, M. L. (2013). Studying ontogenetic trajectories using resampling methods and landmark data. Hystrix, the Italian Journal of Mammalogy, 24(1), 67-73.

Simpson, G. G. (1945). The principles of classification and a classification of Mammals. Bulletin of the American Museum of Natural History, 85, 16-350.

Smith, J. M., Burian, R., Kauffman, S., Alberch, P., Campbell, J., Goodwin, B., Lande, R., Raupe, D., & Wolpert, L. (1985). Developmental constraints and evolution: a perspective from the Mountain Lake conference on development and evolution. The Quarterly Review of Biology, 60(3), 265-287.

Steppan, S. J., & Schenk, J. J. (2017). Muroid rodent phylogenetics: 900-species tree reveals increasing diversification rates. PloS One, 12, e0183070.

Swanson, M. T., Oliveros, C. H., & Esselstyn, J. A. (2019). A phylogenomic rodent tree reveals the repeated evolution of masseter architectures. Proceedings of the Royal Society B: Biological Sciences, 286, 20190672.

Swiderski, D. L., & Zelditch, M. L. (2013). The complex ontogenetic trajectory of mandibular shape in a laboratory mouse. Journal of Anatomy, 223, 568–580.

Tullberg, T. (1899). Ueber das System der Nagethiere: eine phylogenetische Studie. Akademische Buchdruckerei.

Uller, T., Feiner, N., Radersma, R., Jackson, I. S. C., & Rago, A. (2020). Developmental plasticity and evolutionary explanations. Evolution & Development, 22, 47–55.

Uller, T., Moczek, A. P., Watson, R. A., Brakefield, P. M., & Laland, K. N. (2018). Developmental bias and evolution: A regulatory network perspective. Genetics, 209(4), 949-966.

Ungar, P. S. (2010). Mammal Teeth: Origin, Evolution, and Diversity. JHU Press.

Webster, M., & Zelditch, M. L. (2005). Evolutionary modifications of ontogeny: heterochrony and beyond. Paleobiology, 31(3), 354-372.

West-Eberhard, M. J. (2003). Developmental Plasticity and Evolution. Oxford University Press.

Wilson, D. E., Mittermeier, R. A., Ruff, S., Martínez-Vilalta, A., & Cavallini, P. (Eds.) (2016). Handbook of the Mammals of the World: Lagomorphs and Rodents I. Barcelona, Lynx Edicions.

Wilson, L. A. B. (2013). Allometric disparity in rodent evolution. Ecology and Evolution, 3, 971–984.

Wilson, L. A. B., & Sánchez-Villagra, M. R. (2010). Diversity trends and their ontogenetic basis: an exploration of allometric disparity in rodents. Proceedings of the Royal Society B: Biological Sciences, 277, 1227–1234.

Wolff, J. O., & Sherman, P. W. (2008). Rodent societies: an ecological and evolutionary perspective. University of Chicago Press.

Wood, A. E. (1965). Grades and clades among rodents. Evolution, 19, 115–130.

Young, R. L., & Badyaev, A. V. (2007). Evolution of ontogeny: linking epigenetic remodeling and genetic adaptation in skeletal structures. Integrative and Comparative Biology, 47, 234–244.

Zelditch, M. L., & Swiderski, D. L. (2011). Epigenetic interactions: the developmental route to functional integration. In Hallgrímsson, B., & Hall, B. K. (Eds), Epigenetics: Linking Genotype and Phenotype in Development and Evolution, 290–316.

Zelditch, Miriam Leah, Calamari, Z. T., & Swiderski, D. L. (2016). Disparate postnatal ontogenies do – not add to the shape disparity of infants. Evolutionary Biology, 43, 188–207.

Zelditch, Miriam Leah, Sheets, H. D., & Fink, W. L. (2003). The ontogenetic dynamics of shape disparity. Paleobiology, 29, 139–156.

Zelditch, Miriam Leah, Swiderski, D. L., Sheets, H. D., & Fink, W. L. (2004). Chapter 14 - Morphometrics and systematics. In Zelditch, Miriam Leah, Swiderski, D. L., Sheets, H. D., & Fink, W. L. (Eds.) Geometric Morphometrics for Biologists, 363–381.

Zelditch, Miriam Leah, Wood, A. R., Bonett, R. M., & Swiderski, D. L. (2008). Modularity of the rodent mandible: Integrating bones, muscles, and teeth. Evolution & Development, 10, 756–768.

Table S1. List of specimens. IRSNB: Institut Royal des Sciences Naturelles de Belgique, Bruxelles. MHNG: Museum d'Histoire Naturelle de Genève. MNHN : Museum National d'Histoire Naturelle, Paris. NMB: Naturhistorisches Museum Basel. uB_BGS: Université de Bourgogne, Biogéosciences, Dijon.

Species	Specimen	Age	Supp. Data
Meriones unguiculatus	uB_BGS-G-K-7J	Juvenile	
Meriones unguiculatus	uB_BGS-G-L-7J	Juvenile	
Meriones unguiculatus	uB_BGS-G-M-7J	Juvenile	
Meriones unguiculatus	uB_BGS-G-N-7J	Juvenile	
Meriones unguiculatus	uB_BGS-G-O-7J	Juvenile	
Meriones unguiculatus	uB_BGS-G-K-14J	Subadult	x
Meriones unguiculatus	uB_BGS-G-L-14J	Subadult	x
Meriones unguiculatus	uB_BGS-G-M-14J	Subadult	x
Meriones unguiculatus	uB_BGS-G-N-14J	Subadult	x
Meriones unguiculatus	uB_BGS-G-O-14J	Subadult	x
Meriones unguiculatus	uB_BGS-G-Dad-1	Adult	
Meriones unguiculatus	uB_BGS-G-Dad-2	Adult	
Meriones unguiculatus	uB_BGS-G-Mom-K	Adult	
Meriones unguiculatus	uB_BGS-G-Mom-L	Adult	
Meriones unguiculatus	uB_BGS-G-Mom-M	Adult	
Meriones unguiculatus	uB_BGS-G-Mom-N	Adult	
Meriones unguiculatus	uB_BGS-G-Mom-O	Adult	
Mesocricetus auratus	uB_BGS-H-C1-7J	Juvenile	
Mesocricetus auratus	uB_BGS-H-C4-7J	Juvenile	
Mesocricetus auratus	uB_BGS-H-C5-7J	Juvenile	
Mesocricetus auratus	uB_BGS-H-C6-7J-1	Juvenile	
Mesocricetus auratus	uB_BGS-H-C6-7J-2	Juvenile	
Mesocricetus auratus	uB_BGS-H-C7-7J	Juvenile	
Mesocricetus auratus	uB_BGS-H-C1-14J	Subadult	x
Mesocricetus auratus	uB_BGS-H-C3-14J	Subadult	x
Mesocricetus auratus	uB_BGS-H-C4-14J	Subadult	x
Mesocricetus auratus	uB_BGS-H-C5-14J	Subadult	x
Mesocricetus auratus	uB_BGS-H-C6-14J-1	Subadult	x
Mesocricetus auratus	uB_BGS-H-C6-14J-2	Subadult	x
Mesocricetus auratus	uB_BGS-H-C7-14J	Subadult	x
Mesocricetus auratus	uB_BGS-H-C1MH-1	Adult	
Mesocricetus auratus	uB_BGS-H-C3MH-1	Adult	
Mesocricetus auratus	uB_BGS-H-C4FH-1	Adult	
Mesocricetus auratus	uB_BGS-H-C6FH-1	Adult	

Species	Specimen	Age	Supp. Data
Microtus arvalis	MHNG-arv_4	Juvenile	
Microtus arvalis	MHNG-arv_5	Juvenile	
Microtus arvalis	MHNG_1477.019	Subadult	x
Microtus arvalis	MHNG_1477.020	Subadult	x
Microtus arvalis	MHNG_1477.021	Subadult	x
Microtus arvalis	MHNG_1477.023	Subadult	x
Microtus arvalis	MHNG_1477.024	Subadult	x
Microtus arvalis	MHNG_1477.025	Subadult	x
Microtus arvalis	MHNG_1477.026	Subadult	x
Microtus arvalis	uB_BGS-M.Arv-Lodesma-1	Adult	
Microtus arvalis	uB_BGS-M.Arv-Lodesma-2	Adult	
Microtus arvalis	uB_BGS-M.Arv-Mayorga-1	Adult	
Microtus arvalis	uB_BGS-M.Arv-Mayorga-2	Adult	
Mus musculus	uB_BGS-M-A-7J	Juvenile	
Mus musculus	uB_BGS-M-B-7J	Juvenile	
Mus musculus	uB_BGS-M-D-7J	Juvenile	
Mus musculus	uB_BGS-M-E-7J	Juvenile	
Mus musculus	uB_BGS-M-G1-7J	Juvenile	
Mus musculus	uB_BGS-M-A-15J	Subadult	x
Mus musculus	uB_BGS-M-B-15J	Subadult	x
Mus musculus	uB_BGS-M-D-15J	Subadult	x
Mus musculus	uB_BGS-M-E-15J	Subadult	x
Mus musculus	uB_BGS-M-G1-15J	Subadult	x
Mus musculus	uB_BGS-M-AMH-1	Adult	
Mus musculus	uB_BGS-M-BMH-1	Adult	
Mus musculus	uB_BGS-M-EMH-1	Adult	
Mus musculus	uB_BGS-M-EMH-2	Adult	
Mus musculus	uB_BGS-M-Mom-A	Adult	
Mus musculus	uB_BGS-M-Mom-B	Adult	
Mus musculus	uB_BGS-M-Mom-G	Adult	
Mus musculus	uB_BGS-M-Mom-E	Adult	
Rattus rattus	MHNG_766.94-1	Juvenile	
Rattus rattus	MHNG_766.94-3	Juvenile	
Rattus rattus	MHNG_766.94-4	Juvenile	
Rattus rattus	MHNG_1613-57	Adult	
Rattus rattus	MHNG_1613-59	Adult	
Rattus rattus	MHNG_1649-94	Adult	
Rattus rattus	MHNG_1649-95	Adult	

Species	Specimen	Age
Oryctolagus cuniculus	IRSNB_1591	Juvenile
Oryctolagus cuniculus	IRSNB_3261	Juvenile
Oryctolagus cuniculus	IRSNB_6255	Juvenile
Oryctolagus cuniculus	IRSNB_6754	Juvenile
Oryctolagus cuniculus	IRNSB_10552	Adult
Oryctolagus cuniculus	IRSNB_13161	Adult
Oryctolagus cuniculus	IRSNB_1590d	Adult
Oryctolagus cuniculus	IRSNB_6575	Adult
Oryctolagus cuniculus	IRSNB_9827	Adult
Funisciurus lemniscratus	MNHN_1960_3884	Juvenile
Funisciurus lemniscratus	MNHN_1961_308	Adult
Funisciurus lemniscratus	MNHN_1981_580	Adult
Funisciurus lemniscratus	MNHN_1981_583	Adult
Funisciurus lemniscratus	MNHN_1990_663	Adult
Muscardinus avellanarius	MNHN_1981-1015	Juvenile
Muscardinus avellanarius	MNHN_1932-4413	Adult
Muscardinus avellanarius	MNHN_1942-390	Adult
Muscardinus avellanarius	MNHN_1966-1032	Adult
Muscardinus avellanarius	MNHN_1981-449	Adult
Capromys pilorides	IRSNB_3281	Juvenile
Capromys pilorides	IRSNB_3282	Adult
Cavia porcellus	IRSNB_7114	Juvenile
Cavia porcellus	IRSNB_39533	Adult
Cavia porcellus	IRSNB_5893	Adult
Cavia porcellus	IRSNB_5894	Adult
Dolichotis patagonum	NMB_8409	Juvenile
Dolichotis patagonum	NMB_13517	Adult
Dolichotis patagonum	NMB_7325	Adult
Dolichotis patagonum	NMB_7647	Adult
Dolichotis patagonum	NMB_7979	Adult

Species	Specimen	Age
Erethizon dorsatum	NMB_13508	Juvenile
Erethizon dorsatum	NMB_1451	Juvenile
Erethizon dorsatum	NMB_6999	Adult
Erethizon dorsatum	NMB_7268	Adult
Erethizon dorsatum	NMB_7729	Adult
Erethizon dorsatum	NMB_872	Adult
Hystrix cristata	NMB_6193	Juvenile
Hystrix cristata	NMB_13309	Adult
Hystrix cristata	NMB_13308	Adult
Hystrix cristata	NMB_13311	Adult
Hystrix cristata	NMB_13313	Adult
Lagostomus maximus	NMB_6560	Juvenile
Lagostomus maximus	NMB_9995	Juvenile
Lagostomus maximus	NMB_13514	Adult
Lagostomus maximus	NMB_13515	Adult
Lagostomus maximus	NMB_5435	Adult
Lagostomus maximus	NMB_7239	Adult
Myocastor coypus	IRSNB_627D	Juvenile
Myocastor coypus	IRSNB_9099	Adult
Myocastor coypus	IRSNB_1773	Adult
Myocastor coypus	IRSNB_627	Adult
Thryonomys swinderianus	NMB_13344	Juvenile
Thryonomys swinderianus	NMB_13327	Adult
Thryonomys swinderianus	NMB_13328	Adult
Thryonomys swinderianus	NMB_13332	Adult
Thryonomys swinderianus	NMB_13349	Adult

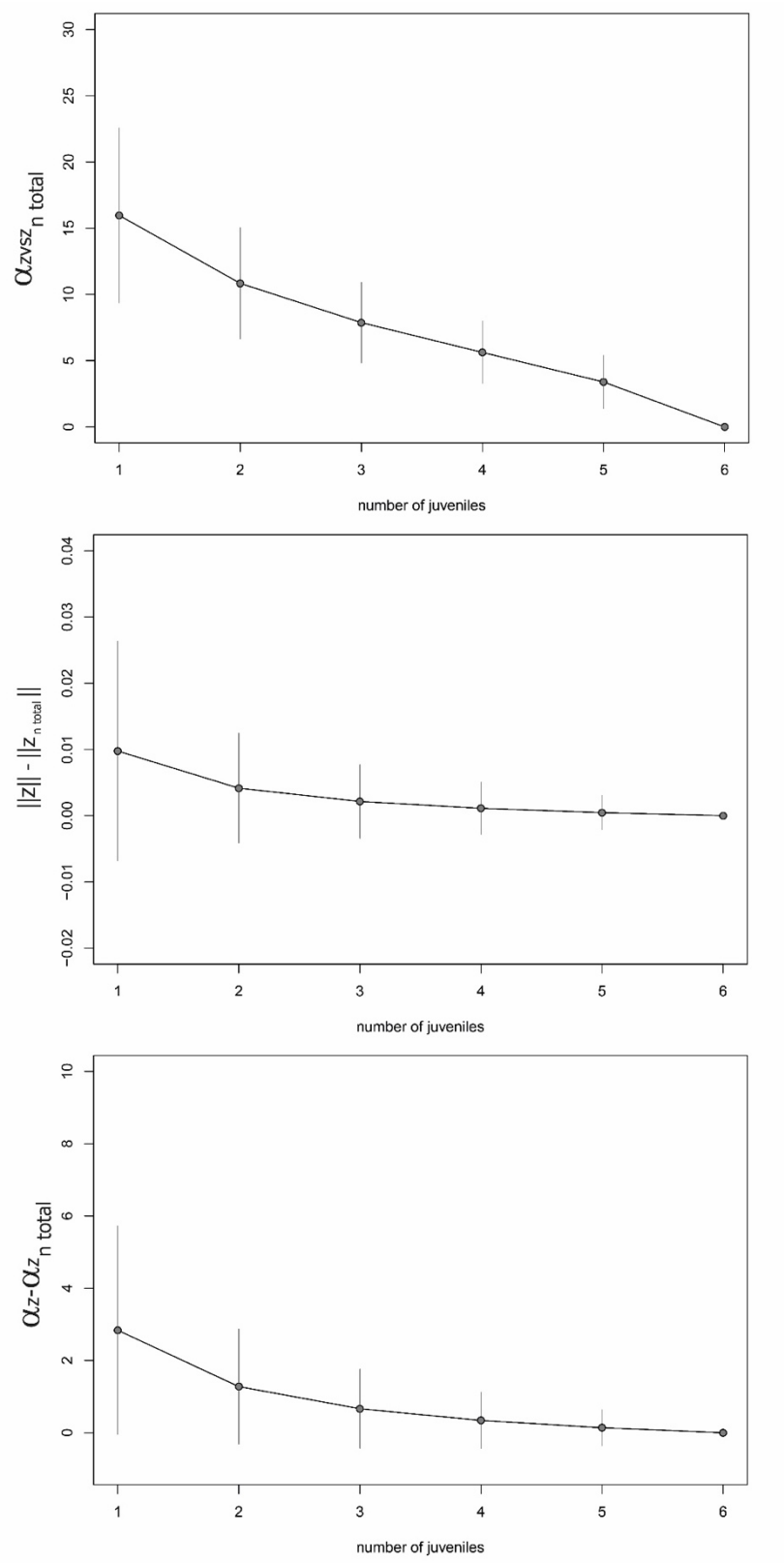

Supplementary figure S1. Effect of the number of sampled juveniles. A) Angle between the postnatal trajectories ***z*** estimated from the complete or the downsampled sets of juveniles. B) Differences in the amount of postnatal changes between the complete and the downsampled sets of juveniles. C) Differences in angles between the ancestral postnatal trajectory ($\bar{\boldsymbol{z}}_{pgls}$) and the species trajectories estimated either with the complete or the downsampled sets of juveniles.

Supplementary Table S2. Effect of the variation in age of juveniles.

Species	alpha*	theta**	prop.norm***
Mus musculus	48.98	13.44	0.39
Mesocricetus auratus	30.74	9.52	0.73
Meriones unguiculatus	29.19	4.91	0.85
Microtus arvalis	42.38	18.06	0.68

*alpha: angle between Adult-Juvenile and Adult-subAdult
**theta: diff. between angles with common trajectory $\bar{\mathbf{z}}_{pgls}$
***Proportion of the norm of the Adult-Juvenile vector

Supplementary Table S3. Disparity (Procrustes variances) of clade × age groups.

suborder	age	disparity
Hystricomorpha	all	0.0169 ± 0.0014
Myomorpha	all	0.0213 ± 0.0018
Hystricomorpha	juvenile	0.0163 ± 0.0020
Myomorpha	juvenile	0.0110 ± 0.0019
Hystricomorpha	adult	0.0149 ± 0.0019
Myomorpha	adult	0.0135 ± 0.0031

Error rate and power of the phylogenetic generalized least-squares using Procrustes sum of squares and residual permutations

Shapes were simulated in the tangent space following its linear approximation (Bookstein 2016; Klingenberg 2020) given the mean shape of our sample and an isotropic variation. This simulation scheme respects the constraints that the Procrustes superimposition imposes on the variation. This is the main difference to the simulations of Adams and Collyer (2018) where multiple traits were simulated with a similar effect on each dimension. Also, our focal tree is half smaller than the tree used in this previous study.

The norm of the simulated shape change was scaled to a certain proportion of the total Procrustes variance (at most 50%). 100 simulations of shape effect and residuals were done and for each of them 100 Brownian evolution of the covariate were simulated. Two kind of covariate were simulated: a continuous one and a three-state character. Analysis with a random binary classification was also realized. Probability of the effect was estimated with phylogenetic GLS within the package geomorph 3.2.1 (Adams et al. 2020) and evaluated using 1000 residual permutations with the package RRPP 0.5.2 (Collyer and Adams 2018). The family-wise error rate was computed on as the proportion of significant pGLS when no covariate effect was simulated and again this error rate was averaged across the 100 shape configurations (Table S4). For each of the three models, the expected FWER is lower than 5%.

Supplementary Table S4. Error rate for the pGLS given the 16 species tree

Effect	fwer	2.5th quantile	97.5th quantile
Quantitative covariate	0.042	0.005	0.08
3-state covariate	0.049	0.01	0.11
Binary class	0.039	0.01	0.08

Power was computed as the proportion of the simulations where the probability was lower than 0.05 and the average across the 100 shape configurations was reported (Figure S2).

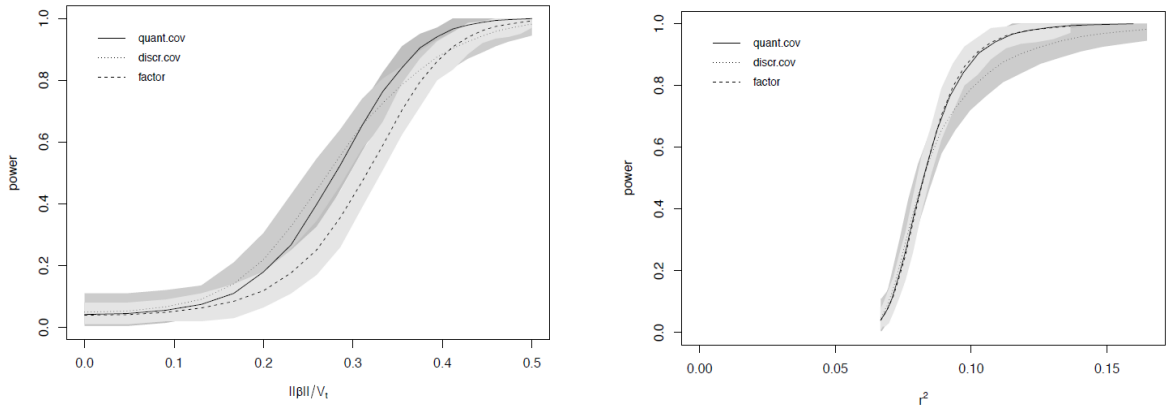

Figure S2. Power of pGLS given the 16 species tree and the three kind of covariate or grouping. X-axis on the left panel reported the ratio of the norm of the effect β (effect to be simulated) to the total variance (the sum of eigenvalues), and the observed r^2 on the right. Shade area represent 95th interval of the 100 shape simulations and lines their averages.
Power reaches 80% for an effect size equal to 0.35 (quantitative covariate), 0.37 (3-state covariate), and 0.39 (binary classification).

Movies S1. Shape changes according to the ancestral estimate of postnatal growth trajectory apply to the estimate of the juvenile mean shape of either the Myomorpha or the Hystricomorpha.

Movies S2. Shape changes according to the effect of the hypselodonty estimated from the pGLS and applied to the Myomorpha mean shape (based on a brachyodont shape).